International Symposium on Impact Engineering 2019

Dynamic compression of 3D printed metallic mesostructures with in-situ X-ray imaging

Martin Jäcklein[1, a *], Konstantin Kappe[1, b], Aron Pfaff[1, c], Marius Bierdel[1, d], Klaus Hoschke[1, e], Matthias Wickert[1, f], Werner Riedel[1, g], Jacob Forster[1, h], Daniel Eakins[2, i], Emilio Escauriza[2, j], Liam Smith[2, k], Alexander Rack[3, l]

[1]Fraunhofer-Institute for High-Speed Dynamics, Ernst-Mach-Institut, EMI, Freiburg, Germany

[2]University of Oxford, Oxford, United Kingdom

[3]European Synchrotron Radiation Facility, Grenoble, France

[a]martin.jaecklein@emi.fraunhofer.de, [b]konstantin.kappe@emi.fraunhofer.de, [c]aron.pfaff@emi.fraunhofer.de, [d]marius.bierdel@emi.fraunhofer.de, [e]klaus.hoschke@emi.fraunhofer.de, [f]matthias.wickert@emi.fraunhofer.de, [g]werner.riedel@emi.fraunhofer.de, [h]jacob.forster@emi.fraunhofer.de, [i]daniel.eakins@eng.ox.ac.uk, [j]emilio.escauriza@seh.ox.ac.uk, [k]liam.smith@eng.ox.ac.uk, [l]alexander.rack@esrf.fr

*corresponding author

Keywords: additive manufacturing, laser beam melting, mesostructures, lattice structures, auxetic structures, dynamic compression, numerical simulation, in-situ X-ray imaging.

Abstract

Additive manufacturing (AM) is an attractive approach for the design and production of complex structures not possible to realize with conventional methods. While the dynamic mechanical response of bulk material is object of extensive investigation, the dynamic behavior of mesostructured material is lacking attention. In this study, a series of different mesostructures, such as lattice and auxetic structures, was designed and additively manufactured in Ti-6Al-4V by laser beam melting (LBM). Dynamic compression tests at velocities around 150 – 360 m/s were conducted at selected samples using a gas-gun. In-situ X-ray imaging provided image data showing an influence of the design of the mesostructure on its failure behavior. Numerical simulations of the impact were compared to the experiments demonstrating a promising accordance. The results enable improved numerical simulation models enhancing their prognostic capacity. Moreover, the findings support the development of design approaches considering the structure-dependent failure behavior.

1. Introduction

In contrast to conventional manufacturing methods like milling or turning, additive manufacturing (AM) offers a broader design freedom. This enables the realization of complex structures on the mesoscale. Examples for these structures are inter alia fine cellular lattice structures. The design and manufacturing of these structures is driven by their ability to feature high mechanical performance such as high strength, high modulus and good energy absorption capacity at a relatively low mass [1]. These characteristics implicate a great potential for the absorption of kinetic energy and can therefore be used in applications like crash absorbing systems in the automotive or aerospace field and blast mitigation in the security or civil protection sector. Moreover, the reduction of resource consumption and building time are welcomed side effects of these structures. However, the manufacturing costs are still high and the reliability of the fabrication process is still challenging. Consequently, the development of working predictive numerical models plays a crucial role. The capability to evaluate design concepts is of fundamental importance in order to optimize structures for their specific use.

Different designs of lattices have been investigated in recent studies [1-7]. However, the focus is on strain rates up to 10^3 s^{-1} or quasi-static loading. Therefore, in some of the simulation models dynamic effects and material failure were not taken into account. Jin et al. [1] investigated the failure and the energy absorption characteristics of different lattices structures. Hereby, the relation between relative density, cell type and energy absorption was studied. Strain rates of 10^3 s^{-1} were analyzed. Imbalzano et al. [2] effectively simulated auxetic sandwich panels under high velocity impact. However, damage of the lattices was not considered and no experimental validation is published so far.

In this paper, we focus on the investigation of several mesostructures under high velocity impact resulting in high strain rates in the range of 10^4 - 10^5 s^{-1}. A couple of homogeneous and gradient lattice structures as well as auxetic mesostructures have been tested. The structural and failure behavior was captured by ultra-high-speed in-situ X-ray imaging [8]. This enables the analysis of the failure behavior like buckling or local and global deformation of various lattice designs. The experimental outcomes allow a validation of the predictions of the numerical simulation results and an improvement of the applied numerical models. Furthermore, this study shows a first approach to influence the location of initial failure.

2. Materials and Methods

In this study, a series of different auxetic and non-auxetic mesostructures was designed. Several auxetic structures based on different unit cell shapes were constructed with homogeneous distributions of identical cells. The auxetic cell geometries were inspired by existing literature [9, 10]. Additionally, cubic space centered lattices have been designed with variations in truss diameter or with a continuous gradient of the truss thickness. All digital information regarding the non-auxetic lattice structures were generated by an in-house developed algorithm enabling the creation of complex lattice structures. The CAD-constructions are based on NURBS splines and smooth transitions between structural members [11]. The cubically designed mesostructures had a volume of 8x8x8 mm³ and were arranged between two plates of 2 mm thickness. Figure 1 (left) illustratively shows a CAD model of a designed mesostructure.

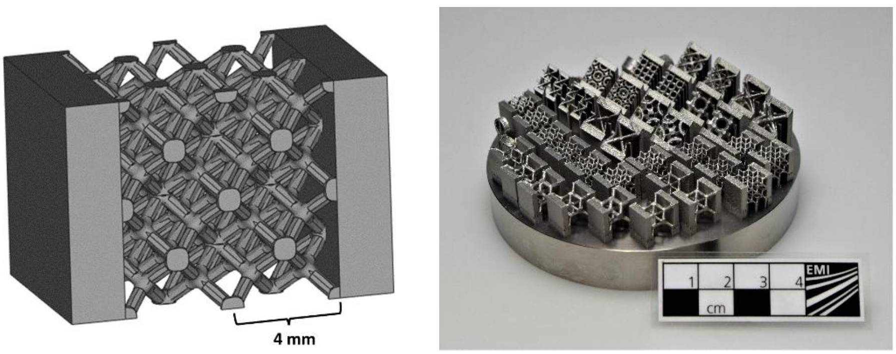

Figure 1 – Left: CAD model of a designed mesostructure. Right: 3D printed metallic mesostructures on the building plate.

The investigated samples were produced by a commercial laser beam melting (LBM) system (EOS M 100) equipped with a 200 W laser unit (YLR-series, CW-laser, wavelength 1070 nm, Gaussian TEM_{00} mode). The titanium alloy Ti-6Al-4V (*particle size distribution* D_{50}*: 39 ± 3 µm*) was processed in 20 µm layers. No heating was applied to the building platform and an argon-based inert gas atmosphere of $O_2 < 0.1$ % was applied in order to avoid oxidation. A shield gas stream flowing over the powder bed was applied to remove any side products arising from the welding process. The samples were built in two orientations; horizontal or diagonal (see Figure 1, right). The production in a vertical orientation is not possible due to manufacturing restrictions. The support structures were removed manually. No heat treatment or other post treatment was applied.

In the test setup, a subset of the printed structures was impacted at velocities around 150 – 360 m/s by an aluminum flyer plate of 5 mm thickness using a gas-gun [12]. Each flyer plate with its polycarbonate sabot had a mass of about 21 g. The samples were mounted on aluminum plates of about 15 g. The impact process was recorded with ultra-high-speed in-situ X-ray imaging [8]. The analysis of the obtained image data was performed with the digital image correlation software GOM Correlate.

3. Results and Discussion

3.1. Experimental

The following analysis focuses on the experiments listed in Table 1. The nominal diameter of the trusses refers to the CAD data. Due to manufacturing tolerances, the real diameters tend to a certain oversize.

Table 1 – Experimental data.

Sample ID	Sample type	Sample mass [g]	Impact velocity [m/s]
1	Structure 1: lattice with trusses of 0.25 mm nominal diameter	1.32	142
2	Structure 2: lattice with trusses of 0.55 mm nominal diameter	1.57	350
3.1	Structure 3: lattice with truss diameter gradient from 0.25 to 0.55 mm	1.47	137
3.2			360
4.1	Structure 4: auxetic structure	0.79	145
4.2			247

In the following figures, impact events for each sample type are displayed in a series of representative images. The impact direction points to the right. With starting deformation of sample 1 (Figure 2) due to the impact, an expansion of the lattice cells orthogonal to the impact direction can be detected. The compressive forces are conducted to the fringe area to a certain extent. This can be explained by the fact that the trusses leading to the fringe are free ends, whereas the trusses in the center are supported by the back plate. This leads to a triangular area in the right center of the sample withstanding the impact force longer. This implies that the behavior of the unit cells is dependent on the boundary conditions. A single unit cell will behave differently than an arrangement of several cells or even the limiting case of an infinite layer of cells. The failure behavior of the sample starts near the impacted side and continues as a cascade through the sample. There seems to be a structural response at low stress amplitudes that is followed by crushing under full impact stresses from the left to the right. In contrast to sample 1, sample 2 (Figure 3) exhibits a lower degree of plastic deformation and therefore a less pronounced triangular zone. However, it is not trivial to deduce and compare an energy absorption capability from the image data. Contrary to the failure behavior of samples 1 and 2, a shock wave passes sample 3.1 (Figure 4) and initiates failure near the non-impact side. Nevertheless, the triangular area can also be observed in this case. Comparing samples 1 and 3.1, it can be stated that the latter undergoes less damage. This suggests that the energy absorption behavior of sample 1 could be superior.

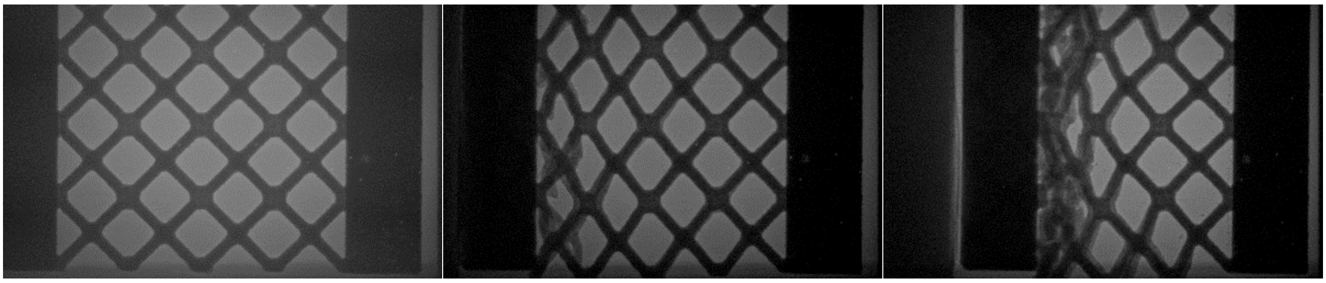

Figure 2 - Sample 1 before (left, t = 0 µs) and during (middle, t = 10 µs and right, t = 26 µs) the impact process of an aluminum flyer plate with an impact velocity of 142 m/s.

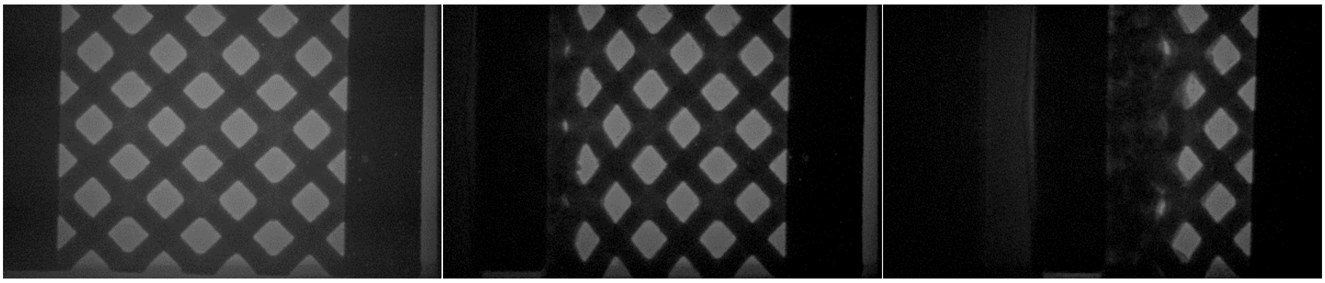

Figure 3 - Sample 2 before (left, t = 0 µs) and during (middle, t = 7 µs and right, t = 23 µs) the impact process of an aluminum flyer plate with an impact velocity of 350 m/s.

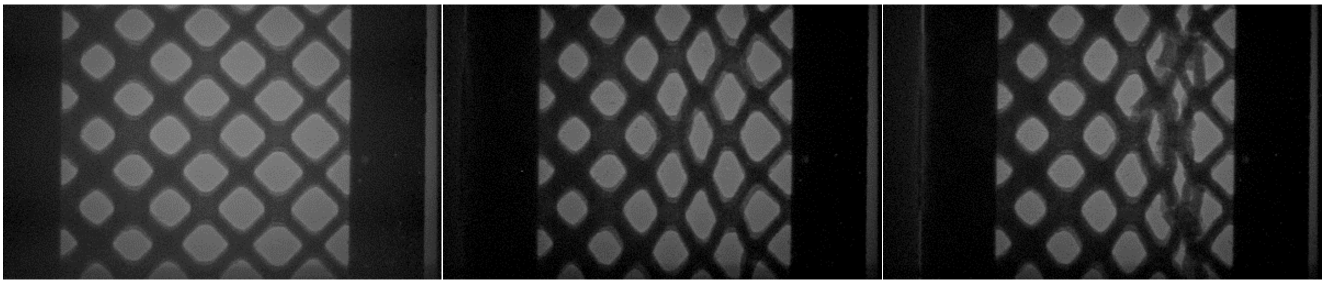

Figure 4 - Sample 3.1 before (left, t = 0 µs) and during (middle, t = 10 µs and right, t = 16 µs) the impact process of an aluminum flyer plate with an impact velocity of 137 m/s.

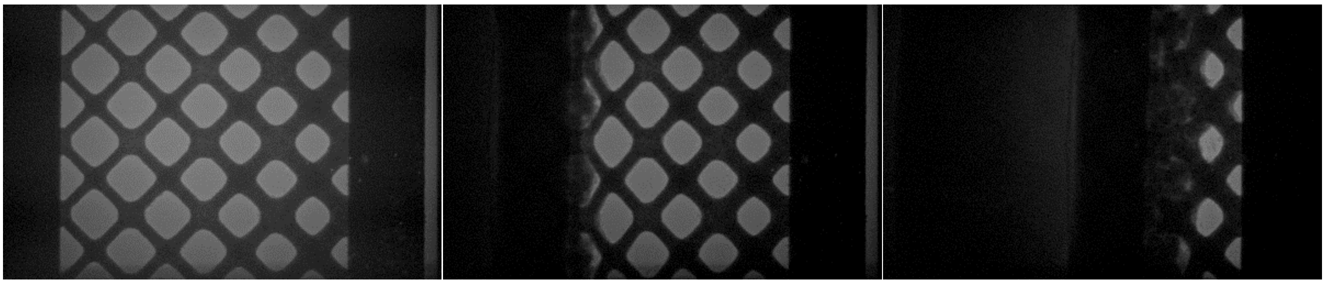

Figure 5 - Sample 3.2 before (left, t = 0 µs) and during (middle, t = 9 µs and right, t = 24 µs) the impact process of an aluminum flyer plate with an impact velocity of 360 m/s.

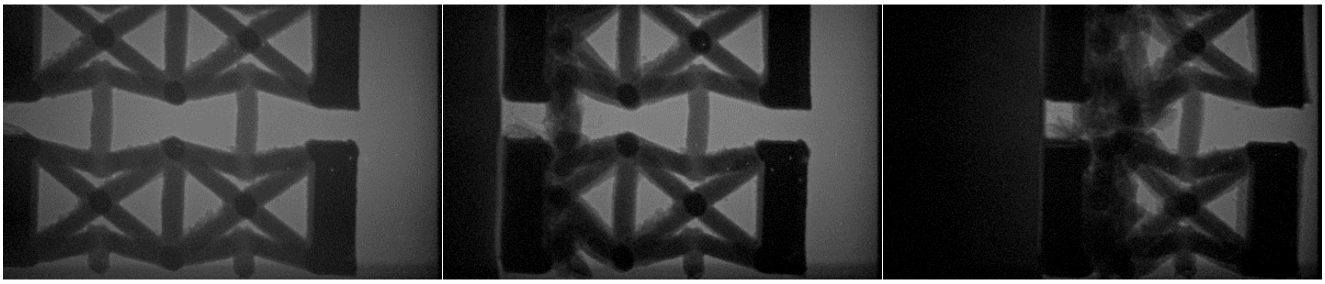

Figure 6 – Sample 4.2 before (left, t = 0 µs) and during (middle, t = 10 µs and right, t = 26 µs) the impact process of an aluminum flyer plate with an impact velocity of 247 m/s.

Sample 3.2 (Figure 5) was impacted inversely to sample 3.1. The failure behavior on the left side is similar to the thin structure of sample 1, on the right side to the thicker structure of sample 2.

Structure 4 (Figure 6) could be proved to exhibit auxetic behavior, meaning contraction of the unit cells in all three dimensions due to compressive forces in one direction. This causes a material densification potentially leading to a higher resistance against compression [13]. However, in this case, it is not obvious from the images whether there is a beneficial effect on the energy absorption behavior due to the structure itself. Contrary to the lattice structures discussed before, the unit cells in this structure type are laterally isolated. This allows each cell to deform individually.

Figure 7 (left) displays the displacement behavior of the front and the back plates, respectively. A source of error in the analysis can be the scale, due to the fact that it has to be set manually in the software. However, this does not affect the qualitative results of the analysis. Small leaps in the displacement curves shown below can be explained by tracking problems of the software and may not be overrated. The curves are cut if the analyzed points are lost before leaving the record window. Missing points in the curves are interpolated.

Looking at the displacement of the front plates, it is obvious that the slope of the curves increases with higher impact velocity. Analyzing the beginning of acceleration of the back plates (Figure 7, right), it can be stated that the displacement behavior of structures 3 and 4 seems to be independent of the impact velocity and the impact direction. For structure 4, the curves for sample 4.1 and 4.2 separate at around 5 µs. In the case of structure 3, the displacement behavior seems to be similar up to 16 µs. This implies that similar low amplitude stress waves pass the structure before the crushing front reaches the back plate.

Comparing the displacement behavior of sample 1 with sample 3.1, it can be observed that despite a slightly higher impact velocity, the increase in velocity of the back plate is quite lower. This confirms the assumption that the performance of structure 1 concerning the damping behavior is better due to a higher degree of plastic deformation. Nevertheless, the behavior of sample 3 impacted from opposite directions demonstrates the possibility to determine the location of first failure by designing structures for specific purposes.

Concerning the samples 2 and 3.2 tested at similar impact velocities, the final velocities of the back plates seem to converge. However, the acceleration characteristics differ considerably. Sample 3.2 exhibits a more delayed but then faster increasing acceleration. This can be related to the gradient characteristics of the structure with thin struts at the front changing to thick struts at the back. At first, the finer structure offering less resistance collapses. Therefore, the transmission of kinetic energy to the back plate is reduced in the beginning. The non-gradient structure of sample 3.2 leads to a steadier transfer of momentum.

The behavior of the auxetic structure 4 cannot be compared directly to the other samples, as the sample mass is approximately just one half. Nevertheless, it can be stated that the structure shows a clear damping effect which needs to be analyzed further.

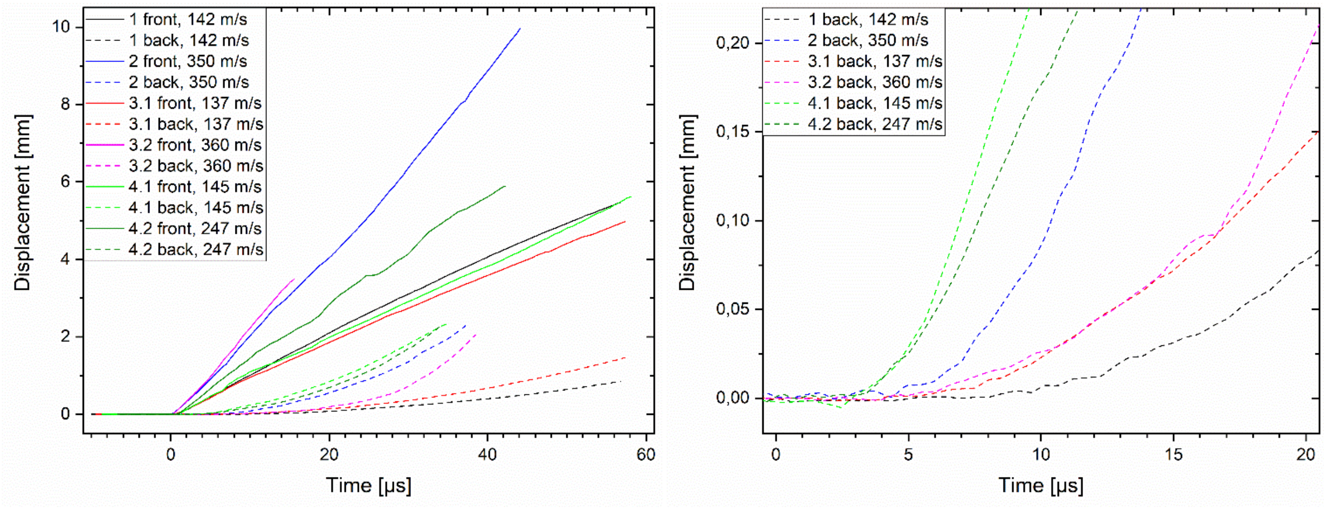

Figure 7 – Displacement of impacted samples analyzed for front (solid lines) and back plates (dashed lines), respectively. The right image is a magnified view of the time range when the acceleration of the back plates starts.

3.2. Simulation

A three-dimensional, numerical model representative of the complex lattice structures was developed using the Altair Radioss explicit finite element code. The model consists of three different components, the flyer plate, the mounting plate and the structure. To minimize the computing time, symmetric boundary conditions were applied. Therefore, only a quarter of the components had to be modeled. The flyer and mounting plate were modeled as 2-D shell elements. Due to the expected deformation of the mounting plate, an elastic-plastic material model was chosen, whereas the flyer was modeled with an elastic material model. For the impacted lattice structures, a more complex material model was used.

Deformation under impact loading is a complex and dynamic process and requires the consideration of strain, strain rates and material failure. Therefore, the Johnson-Cook (JC) constitutive material model was used to model the material of the lattice structures. Material failure was taken into account by a simplified damage model, where damage occurred when a critical fracture strain was reached. In this case, the affected element was deleted. Previous implementation of the JC failure model showed a premature damage occurrence and therefore a great discrepancy in the simulation results. Furthermore, an equation of state was necessary to successfully describe the material model due to the fact that ductile material is impacted at significant high speed (>120 m/s) [14]. Therefore, the Mie-Grüneisen equation of state was taken into account. The material parameters of Ti-6Al-4V for the JC material model and the Mie-Grüneisen equation of state were taken from existing literature [15, 16].

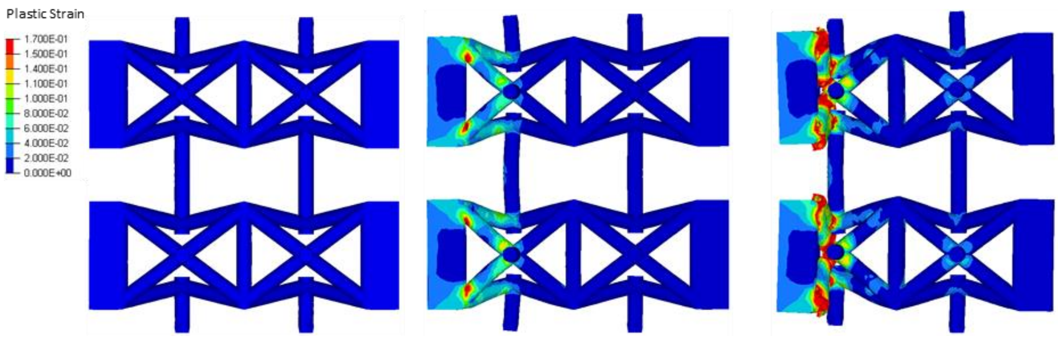

Figure 8 - Simulation of plastic strain of the impacted auxetic lattice structure 4. with an impact velocity of 145 m/s corresponding to sample 4.1 at t = 0 µs (left), t = 4 µs (middle) and t = 17 µs (right).

Exemplarily, Figure 8 shows the simulation results of the auxetic lattice structure 4 with an impact velocity of 145 m/s corresponding to sample 4.1. Failure occurred mainly in the connection from the lattices to the front plate as well as in the first connection point between the lattices. Also, the auxetic effect of the cells in the first layer can be observed. These results match with the experimental results. Furthermore, the time dependent displacements of the impacted front and non-impacted back plate of the lattices were investigated. The displacement of the lattice structure 4 at impact velocity of 145 m/s of both experiment and simulation are shown in Figure 9. It can be seen that the resulting displacements of the simulation model do not totally agree with the results of the experiment. In particular, the displacement of the non-impacted side of lattice structures shows smaller values. It can be assumed that the difference is mainly due to the material loss of the lattice structure. In the simulation, damaged elements were deleted from the model. In case of impact, high strains occur and many elements satisfy the failure criterion and are deleted. During the simulation, 6 % of the elements were deleted due to the simplified failure model in comparison to the JC damage model, where approximately 20 % of the elements were erased. It is known that the erasure of an element often leads to underestimation of reaction forces and non-physical failure patterns [17]. For example, the reaction forces could not be transferred by the lattices from the impacted side to the non-impacted side of the structure. The resulting displacement of the non-impacted side confirms this assumption.

For the simulation, different refined meshes were used. Although a fine mesh is required to provide a convergent solution, it implies higher computational costs. As a result of high deformations of the elements, a significant decrease of the time step occurred and the computing time increased to an unwanted level.

Furthermore, it is to mention that geometrical variation due to manufacturing tolerances of the LBM process have not been considered. Also, the JC material and damage parameters, which had been taken from the literature, were determined based on conventionally manufactured Ti-6Al-4V. The comparison between the experiment and the simulation results showed that the proper material characteristics of additively manufactured Ti-6Al-4V need to be investigated. Especially, the material and failure characteristics of fine lattices need to be analyzed.

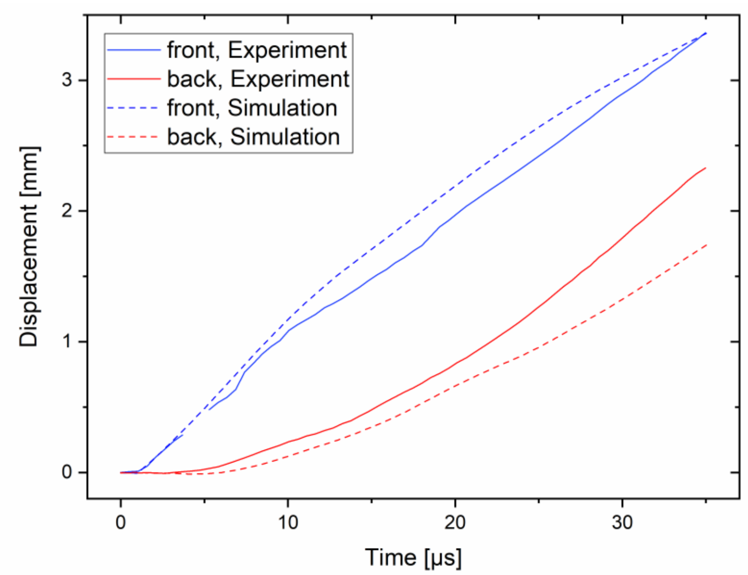

Figure 9 - Time-displacement-curve of front and back plate of lattice structure 4.1.

4. Conclusions

This study showed that the design of a mesostructure has an influence on the characteristics of its energy absorption and its failure behavior. For this purpose, a selection of homogeneous, gradient and auxetic mesostructures was analyzed under impact velocities between 140 m/s and 360 m/s. By analyzing the images, the time dependent displacements of the front and back plates of the structures were investigated. Whereas the homogeneous lattice structures with different truss diameters showed a similar structural behavior under impact, the lattice structure with truss diameter gradient showed that it is possible to influence the location of initial failure under high velocity impact. In addition, it could be concluded that the failure behavior is dependent on the boundary conditions of the mesostructure. An auxetic effect could be proven at an auxetic mesostructure under two impact velocities up to 250 m/s.

Besides the experimental testing, simulations of the mesostructures were realized. Although the simulation results show the correct tendency of the structural and failure behavior of the lattice structures, there are discrepancies caused by element erasure and imprecise material parameters. Therefore, material characteristics of LBM manufactured Ti-6Al-4V need to be determined. In particular, the characteristics of thin trusses and the influence of scaling should be investigated.

It needs to be mentioned that the variety of different structures and impact velocities was restricted in this work. For further predications of the characteristics of different mesostructures, more systematic studies at different impact velocities will be necessary. Thereby, the impact velocities can be determined where shockwave effects have a significant impact on the structural behavior of thin truss diameter mesostructures. As well, the strain rate dependent characteristics of the lattices can be investigated. These results will help to obtain an effective simulation model. Furthermore, more designs of lattices should be analyzed. Thereby, different gradients in truss diameter of the lattices can be applied to vary the location of initial failure. An improved understanding of the correlation between structural design and failure behavior would enable the simulation-based design of optimized structures for specific applications.

Acknowledgements

We acknowledge the European Synchrotron Radiation Facility for provision of synchrotron radiation facilities and we would like to thank Dr. Alexander Rack for assistance in using beamline ID 19.

References

[1] N. Jin, F. Wang, Y. Wang, B. Zhang, H. Cheng, H. Zhang, Failure and energy absorption characteristics of four lattice structures under dynamic loading, Materials and Design 169 (2019) Art. No. 107655.

[2] G. Imbalzano, P. Tran, T. D. Ngo, P. V. S. Lee, Three-dimensional modelling of auxetic sandwich panels for localised impact resistance, Journal of Sandwich Structures & Materials 19(3), (2017), 291–316.

[3] S. McKown, Y. Shen, W. K. Brookes, C. J. Sutcliffe, W. J. Cantwell, G. S. Langdon, G. N. Nurick, M. D. Theobald, The quasi-static and blast loading response of lattice structures, International Journal of Impact Engineering 35 (2008), 765-810.

[4] T. Tancogne-Dejean, A. B. Spierings, D. Mohr, Additively-manufactured metallic micro-lattice materials for high specific energy absorption under static and dynamic loading, Acta Materialia 116 (2016), 14-28.

[5] L. Xiao, W. Song, C. Wang, H. Tang, Q. Fan, N. Liu, J. Wang, Mechanical properties of open-cell rhombic dodecahedron titanium alloy lattice structure manufactured using electron beam melting under dynamic loading, International Journal of Impact Engineering 100 (2017), 75-89.

[6] D. S. J. Al-Saedi, S. H. Masood, M. Faizan-Ur-Rab, A. Alomarah, P. Ponnusamy, Mechanical properties and energy absorption capability of functionally graded F2BCC lattice fabricated by SLM, Materials and Design 144 (2018), 32-44.

[7] R. Vrána, D. Paloušek, D. Koutný, O. Koukal, T. Zikmund, P. Krejčí, Impact resistance of lattice structure made by Selective laser melting technology, Modern Machinery Science Journal, (2015).

[8] E. M. Escauriza, M. P. Olbinado, M. E. Rutherford, D. J. Chapman, J. C. Z. Jonsson, A. Rack, D. E. Eakins, Ultra-high-speed indirect X-ray imaging system with versatile spatiotemporal sampling capabilities, Applied Optics 57, No. 18 (2018).

[9] S. Babaee, J. Shim, J. C. Weaver, E. R. Chen, N. Patel, K. Bertoldi, 3D soft metamaterials with negative Poisson's ratio, Advanced Materials 25, No.36 (2013), 5044-5049.

[10] J. C. Á. Elipe, A. D. Lantada, Comparative study of auxetic geometries by means of computer-aided design and engineering, Smart Materials and Structures 21 (2012), Art. No. 105004.

[11] K. Hoschke, A. Pfaff, L. Fleig, M. Bierdel, M. Jäcklein, W. Riedel, S. Hiermaier, A parametric mesostructural approach for robust design of additive manufacturing parts, 4th Fraunhofer Direct Digital Manufacturing Conference DDMC (2018).

[12] D. E. Eakins, D. J. Chapman, X-ray imaging of subsurface dynamics in high-Z materials at the Diamond Light Source, Review of Scientific Instruments 85 (2014).

[13] A. Alderson, A triumph of lateral thought: Imagine stretching elastic and seeing it get fatter rather than thinner. It may sound bizarre, but this property is what makes auxetic materials potentially so useful, Chemistry & Industry (1999), 384–391.

[14] H. K. Farahani, M. Ketabchi, and Sh. Zangeneh, Determination of Johnson–Cook plasticity model parameters for Inconel718, Journal of Materials Engineering and Performance 11 (2017).

[15] X. Wang, J. Shi, Validation of Johnson-Cook plasticity and damage model using impact experiment, International Journal of Impact Engineering 60 (2013).

[16] D. Lesuer, Experimental investigations of material models for Ti-6Al-4V titanium and 2024-T3 aluminum, FAA report, DOT/FAA/AR-00/25 (2000).

[17] W. Hu, C. T. Wu, S. Hayashi, The Immersed Smoothed Particle Galerkin method in LS-Dyna for material failure analysis of fibre-reinforced solid structures, 15th International LS-Dyna Users Conference (2018).